

Symmetry protected topological phases characterized by isolated exceptional points

S. Lin,¹ L. Jin,^{1,*} and Z. Song^{1,†}

¹*School of Physics, Nankai University, Tianjin 300071, China*

Exceptional point (EP) associated with eigenstates coalescence in non-Hermitian systems has many exotic features. The EPs are generally sensitive to system parameters, here we report symmetry protected isolated EPs in the Brillouin zone (BZ) of a two-dimensional non-Hermitian bilayer square lattice; protected by symmetry, the isolated EPs only move, merge, and split in the BZ. The average values of Pauli matrices under the eigenstate of system Bloch Hamiltonian define a real planar vector field, the topological defects of which are isolated EPs associated with vortices. The winding number characterizes the vortices and reveals the topological properties of the non-Hermitian system. Different topological phases correspond to different EP configurations, which are unchanged unless topological phase transition occurs accompanying with the EPs merging or splitting.

I. INTRODUCTION

Non-Hermitian physics has been extensively investigated in both theoretical and experimental aspects [1–16]. In contrast to phase transition in Hermitian systems, exceptional points (EPs) as non-Hermitian critical points are associated with the coalescence of eigenstates [17–20]. EPs support many novel phenomena, including power oscillation [21], square-root frequency dependence [22–24], and gap protected long-range entangled state [25]. The eigenstate flips [26–31] and geometric phases imprinted [32–35] when encircling EPs for integer circles reveal the exotic topology of EPs [36–38]. The non-Hermitian topological system enables novel interface states in quasi-one-dimension and beyond [39–69]. The topological interface states are classified by two winding numbers originated from the complex magnitude and the varying direction of an effective magnetic field [55]. The Chern number and the vorticity that associated with the eigenstates and the energy band are topological invariant [70]. For the breakdown of conventional bulk-boundary correspondence, the exotic bulk-edge correspondence is developed [71–74]; the importance of chiral inversion symmetry for the conventional bulk-boundary correspondence is revealed [75]. Non-Hermitian topological phases and EP rings/surfaces protected by symmetries are investigated [76–79]; the important application includes the topological lasing [80–84].

Recently, topological gapless systems, which are related to diabolic points (DPs) [85], have emerged as a new frontier in physics [86–104]. As a joint of two quantum phases, topological gapless systems have band structures with band touching points (BTPs) in the momentum space, where these kinds of nodal points appear as topological defects in an auxiliary vector field [89, 97]. These points are unremovable due to symmetry protection until a pair of them meet and annihilate together [105]. In general, the EPs of a two-dimensional non-

Hermitian system form a loop, referred as an exceptional ring [27, 106–108]. A natural question is whether there exist isolated EPs in the momentum space which have similar topological characteristics to nodal points in topological gapless systems.

In this paper, we show that topological nature of BTPs in the Brillouin zone is determined by the topological defects of a real vector field $\mathbf{F}(\mathbf{k})$ mapped from the Bloch Hamiltonian. $\mathbf{F}(\mathbf{k})$ is composed by the average values of Pauli matrices in non-Hermitian systems in contrast to an effective magnetic field in Hermitian systems, a winding number based on which characterizes the vortices at EPs as topological charges. While, another winding number associated with the energy $\mathbf{E}(\mathbf{k})$ characterizes the topology of band coalescence and the chirality of EPs. Moreover, BTPs are protected by system symmetries and their configurations characterize different topological phases. DPs split to pairs of EPs when non-Hermiticity is introduced; EPs inherit half-integer vortices from their parent DPs; topological phase transitions occur associated with the creation of new configurations when EPs (DPs) merge or split. Topology of EPs (DPs) is characterized through topological invariant: the winding numbers 0 or $\pm 1/2$ (0 or ± 1). Our findings are elucidated through a bilayer square lattice.

II. BILAYER SQUARE LATTICE

We consider a tight-binding bilayer square lattice [Fig. 1(a)], typically describing the dissipative ultracold atomic gas in optical lattices [109–114]. The Hamiltonian has the form $H = \sum_{\lambda=1}^2 H_{\lambda} + H_T$, where the intralayer term is

$$\begin{aligned}
 H_{\lambda} = & \sum_{j,l=1}^N [J(|\lambda, j, l\rangle (\langle \lambda, j+1, l| + \langle \lambda, j, l+1|) \\
 & + t(-1)^{\lambda+j+l} \sum_{\nu=\pm 1} |\lambda, j, l\rangle \langle \lambda, j+1, l+\nu| + \text{h.c.}] \\
 & + i\gamma(-1)^{\lambda+j+l} |\lambda, j, l\rangle \langle \lambda, j, l|, \quad (1)
 \end{aligned}$$

* jinliang@nankai.edu.cn

† songtc@nankai.edu.cn

and the interlayer term is $H_T = T |1, j, l\rangle \langle 2, j, l| + \text{h.c.}$; $\lambda = 1$ (2) is the index that labels the upper (lower) layer, and (j, l) is the in-plane site index. In Fig. 1(a), J and T denote the intralayer and interlayer hoppings; t and γ are the diagonal couplings and staggered losses. Different sublattices have different losses γ_A and γ_B due to the environment interactions. After a removal of universal loss $(\gamma_A + \gamma_B)/2$, the losses are equivalently described by the balanced gain and loss $\gamma = (\gamma_A - \gamma_B)/2$.

The translational symmetry ensures that the Hamiltonian H can be represented as the summation of a series of 2×2 matrices under the basis $|\phi(k_x, k_y)\rangle_{A(B)} = \sum_{j,l=1}^N (1/N) e^{i(k_x j + k_y l)} |\lambda_{A(B)}, j, l\rangle$, where $k_x = 2n_x \pi/N$, $k_y = 2n_y \pi/N$ with $n_x, n_y \in [1, N]$, and states $|\lambda_A, j, l\rangle$ and $|\lambda_B, j, l\rangle$ are the position states of sublattices A and B with layer labels $\lambda_A = [3 + (-1)^{j+l}]/2$ and $\lambda_B = [3 - (-1)^{j+l}]/2$.

The Hamiltonian H in real space is rewritten as the summation of Bloch Hamiltonians $h(k_x, k_y)$ in the momentum space

$$H = \sum_{k_x, k_y} h(k_x, k_y) \equiv \sum_{k_x, k_y} \mathbf{B}(\mathbf{k}) \cdot \vec{\sigma} = \sum_{k_x, k_y} B_x \sigma_x + B_y \sigma_z, \quad (2)$$

describing an ensemble of non-interacting spin one-half particles in a two-component complex magnetic field is $\mathbf{B}(\mathbf{k}) = (B_x, B_y, 0)$ with

$$\begin{cases} B_x = 2J(\cos k_x + \cos k_y) + T \\ B_y = 4t \cos k_x \cos k_y + i\gamma \end{cases}, \quad (3)$$

and $\vec{\sigma} = (\sigma_x, \sigma_z, \sigma_y)$ is a vector of Pauli matrices with $\sigma_x = |\phi\rangle_A \langle \phi|_B + |\phi\rangle_B \langle \phi|_A$, $\sigma_y = -i |\phi\rangle_A \langle \phi|_B + i |\phi\rangle_B \langle \phi|_A$, and $\sigma_z = |\phi\rangle_A \langle \phi|_A - |\phi\rangle_B \langle \phi|_B$ [115]. The $\mathbf{B}(\mathbf{k})$ field is invariant under interchanging of k_x and k_y . The BTPs are at $(k_{cx}, \pm\pi/2)$ and $(\pm\pi/2, k_{cy})$, where $|k_{cx(cy)}| = \cos^{-1} [(-T \pm \gamma) / (2J)]$; the BTPs are EPs (DPs) for $\gamma \neq 0$ ($\gamma = 0$).

III. SYMMETRY

Discrete symmetries play a crucial role in characterizing topological phases [116]. Here, t breaks the inversion symmetry and γ breaks the time-reversal symmetry of the bilayer square lattice, but H has a chiral symmetry $\chi H(J, T, \gamma, t) \chi^{-1} = -H(J, T, \gamma, t)$. The chiral operator $\chi = UC_4$ is a combination of a Z_2 gauge transformation U and a 90 degrees rotation C_4 . The Z_2 gauge transformation $U |\lambda_{A(B)}, j, l\rangle = (-1)^{\lambda+j+l} |\lambda_{A(B)}, j, l\rangle$ changes the system Hamiltonian $H(J, T, \gamma, t)$ into $H(-J, -T, \gamma, t)$. The chiral symmetry instead of time-reversal symmetry or inversion symmetry ensures the Bloch Hamiltonian including only two Pauli matrices [96].

The mirror-reflection in the x and y directions (M_x and M_y), the translation of one site in the x and y directions

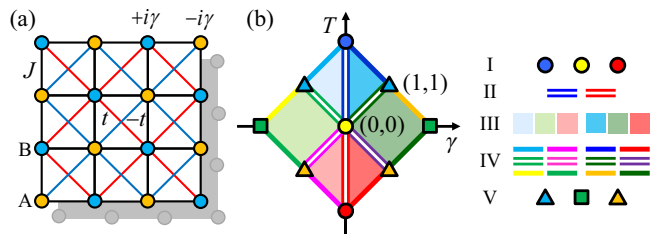


FIG. 1. (a) Schematic of the bilayer square lattice. The intra-sublattice hoppings have opposite signs t (red) and $-t$ (blue). The shadowed lattice indicates the lower layer with $(\gamma, t) \rightarrow (-\gamma, -t)$ in contrast to the upper layer. (b) Phase diagram of the bilayer square lattice in the γ - T plane for $|T \pm \gamma| \leq 2$. Twenty-six topological phases exhibit five types of winding number distributions of BTPs as listed in Table I.

TABLE I. Five types of BTP distributions.

$w_{I,II}$	I	II	III	IV	V
$\{0, \pm 1/2, \pm 1\}$	$\{4, 0, 0\}$	$\{0, 0, 8\}$	$\{0, 16, 0\}$	$\{4, 8, 0\}$	$\{8, 0, 0\}$

(T_x and T_y), the 90 degrees rotation (C_4), and the upper and lower layer interchange (Λ) all change the Hamiltonian $H(J, T, \gamma, t)$ into $H(J, T, -\gamma, -t)$. Therefore, H is invariant under a combination of any two of the above listed operations and leads to (Appendix A)

$$h(k_x, k_y) = h(\pm k_{x(y)}, \pm k_{y(x)}). \quad (4)$$

Therefore, the number of EPs (DPs) in the bilayer lattice is protected by these symmetries, being invariant unless topological phase transition occurs when EPs (DPs) merge or split in the non-Hermitian (Hermitian) bilayer lattice.

Notably, the non-Hermitian bilayer square lattice $H(J, T, \gamma, t)$ does not have either \mathcal{PT} symmetry or \mathcal{CT} symmetry (charge-conjugation symmetry in Ref. [51]) in the situation that $t \neq 0$. The operators \mathcal{C} is defined as $\mathcal{C} |\lambda_{A(B)}, j, l\rangle = (-1)^{0(1)} |\lambda_{A(B)}, j, l\rangle$ [117], \mathcal{T} is defined as $\mathcal{T} i \mathcal{T}^{-1} = -i$, and \mathcal{P} is defined as $\mathcal{P} |\lambda_{A(B)}, j, l\rangle = |\lambda_{A(B)}, N+1-j, l\rangle$ or $|\lambda_{A(B)}, j, N+1-l\rangle$. In the absence of diagonal coupling ($t = 0$), the system satisfies both \mathcal{PT} symmetry $[(\mathcal{PT}) H(J, T, \gamma, t) (\mathcal{PT})^{-1} = H(J, T, \gamma, t)]$ and \mathcal{CT} symmetry $[(\mathcal{CT}) H(J, T, \gamma, t) (\mathcal{CT})^{-1} = -H(J, T, \gamma, t)]$ [117]. \mathcal{PT} symmetry leads to the spectrum being real or being conjugate pairs. \mathcal{CT} symmetry requires the eigen energies appearing in pairs with opposite real parts and identical imaginary parts. Thus, the spectrum under \mathcal{PT} symmetry and \mathcal{CT} symmetry is purely real or purely imaginary.

The system is inversion symmetric and time-reversal symmetric when $t = \gamma = 0$ [70, 118]. The inversion symmetry changes the sign of the momentum and interchanges the upper and lower layers.

IV. TOPOLOGICAL INVARIANTS OF EP

$h(k_x, k_y)$ includes only two Pauli matrices and commutes with the third one, we employ a planar vector field $\mathbf{F}(\mathbf{k}) = (F_x, F_y)$ to characterize the topology of $h(k_x, k_y)$. The zero energy band degeneracy $E_{\pm} = \pm\sqrt{B_x^2 + B_y^2} = 0$ implies that the expectation value of $h(k_x, k_y)$ under its eigenstate is zero, i.e., $\langle h(k_x, k_y) \rangle = B_x \langle \sigma_x \rangle + B_y \langle \sigma_z \rangle = 0$; therefore, $B_x = B_y = 0$ ($\langle \sigma_x \rangle = \langle \sigma_z \rangle = 0$) at DPs (EPs) in Hermitian (non-Hermitian) system. The expectation values of the two Pauli matrices compose the planar vector field

$$\mathbf{F}(\mathbf{k}) = (\langle \sigma_x \rangle, \langle \sigma_z \rangle), \quad (5)$$

for non-Hermitian system instead of $\mathbf{F}(\mathbf{k}) = (B_x, B_y)$ for Hermitian system [96, 97]. EPs are protected by symmetry, exhibiting similar behaviors as DPs in Hermitian lattices and being topologically stable. Moreover, EPs can map to the topological defects of the manifold $\mathbf{F}(\mathbf{k})$, at which $\mathbf{F}(\mathbf{k})$ approaches zero with vortex or antivortex structures.

A topological invariant characterizes the topological property of $\mathbf{F}(\mathbf{k})$

$$w_I = \oint_C \frac{d\mathbf{k}}{2\pi} \left(\hat{F}_x \nabla \hat{F}_y - \hat{F}_y \nabla \hat{F}_x \right), \quad (6)$$

where $\hat{F}_{x(y)} = F_{x(y)} / \sqrt{F_x^2 + F_y^2}$ and $\nabla = \partial / \partial \mathbf{k}$. The integral is performed in the k_x - k_y plane along a closed loop C ; $2\pi w_I$ accounts the varying direction of vector field $\mathbf{F}(\mathbf{k})$. The (both eigenstates yielding identical) winding number w_I describes the vortices with topological charges [70, 108] at EPs and is in parallel to the winding number that originated from the generalized Berry phase [55, 103, 108].

Moreover, the topology of BTP can be determined by winding numbers w_I via the planar vector fields $\mathbf{F}(\mathbf{k})$. By means of w_I , the BTP is classified into four types:

(i) Semi-Dirac point: $H(\mathbf{k})$ is Hermitian and semi-Dirac point possesses an anisotropic dispersion of linear and quadratic dispersions along two orthogonal directions [119–123]. It has winding number $w_I = 0$ and can split into two Dirac points ($w_I = \pm 1$) when changing parameters without breaking any symmetries [124].

(ii) Dirac point: $H(\mathbf{k})$ is also Hermitian and the dispersion is linear along all directions around the Dirac point, but the vector field $\mathbf{F}(\mathbf{k})$ owns a vortex ($w_I = +1$) or an antivortex ($w_I = -1$) with opposite topological charges [125–127]. In the presence of non-Hermiticity, each Dirac point splits into two normal EPs with identical half-integer vortices as in (iii) [128–130]; in contrast, the Dirac point can split into two Weyl points in Hermitian systems with breaking inversion or time-reversal symmetry [118, 131–138].

(iii) Normal EP: The winding numbers of normal EPs are $w_I = \pm 1/2$; it indicates that EPs inherit one-half vortices from their parent Dirac points with $w_I = \pm 1$

[96, 97]. The dispersion is square-root along any direction near the normal EPs.

(iv) Hybrid EP: two normal EPs with opposite vortices can merge into a hybrid EP. In this situation, the winding number of EP is changed from $\pm 1/2$ to 0. Different from that of a semi-Dirac point [119–123], hybrid EP also has an anisotropic dispersion with square-root (linear) dispersions along two orthogonal directions [70].

While, in parallel to w_I , another winding number is defined as

$$w_{II} = \oint_C \frac{d\mathbf{k}}{2\pi} \left(\hat{E}_x \nabla \hat{E}_y - \hat{E}_y \nabla \hat{E}_x \right), \quad (7)$$

with $\mathbf{E}(\mathbf{k}) = (E_x, E_y)$ being the band energy $E = \pm\sqrt{B_x^2 + B_y^2}$ in the complex plane, and $\hat{E}_x = \text{Re}(E)/|E|$, $\hat{E}_y = \text{Im}(E)/|E|$, which characterizes the topology of EPs on another aspect. Both two bands yield identical w_{II} due to chiral symmetry. w_{II} differs from w_I and characterizes the topology of band coalescence [55, 70], reveals the vorticity of complex Riemann surface band structure [28–30], and reflects the chirality of normal EPs [33–36, 139]. Each of the two bands accumulates Berry phase $\pm\pi$ when encircling EPs for two circles; the \pm sign in front determines the opposite chiralities of EPs [19, 20, 26, 33, 35] as a result of the square-root type Riemann sheet. The merge of EPs with opposite chiralities creates DP or hybrid EP [36, 70]. The winding number is $w_{II} = \pm 1/2$ (0) for normal EP (DP and hybrid EP).

V. TOPOLOGICAL PHASES

H is invariant under arbitrary two combinations of the mirror reflection, the translation, the 90 degrees rotation, and the layer interchange. Symmetries protect the Bloch Hamiltonian $h(k_x, k_y)$, being invariant under substitution $(k_x, k_y) \rightarrow (\pm k_{x(y)}, \pm k_{y(x)})$, and also protect the number of BTPs (DPs and EPs) with vortex structures. The BTPs can move but cannot be removed as system parameters varying except when they merge or split associated with a topological phase transition and the creation of a new BTP configuration. The BTP configuration (Figs. 2 and 3) characterizes the topological phases of bilayer square lattice, while the phase diagram is depicted in Fig. 1(b).

The system is Hermitian at $\gamma = 0$, being time-reversal symmetric without inversion symmetry ($t \neq 0$). The time-reversal symmetry requires DPs at $\pm k$ with identical winding number [93, 132]. Eight DPs may exist due to the symmetry protection. They locate and move along the $|k_{x(y)}| = \pi/2$ lines; their locations satisfy a fourfold rotational symmetry (C_4 symmetry) with respect to the axis that perpendicular to the k_x - k_y plane, being mirror-reflection-symmetric about $k_{x(y)} = 0$ and $k_x = \pm k_y$ [136]. Eight DPs merge into four at $|T| = 0$ and $2J$ [93, 131]. Top panel of Fig. 2 shows the DP configurations.

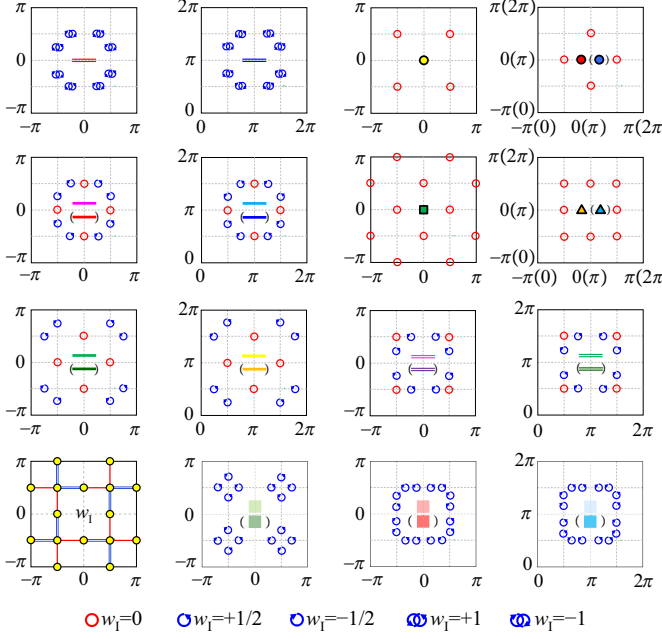


FIG. 2. Schematic of BTP configurations of w_I for the topological phases in Fig. 1(b). The horizontal (vertical) axis is k_x (k_y). The blue arrows and red circles represent $w_I = \pm 1/2$, ± 1 and 0 . w_I of the Hermitian (non-Hermitian) bilayer lattice is shown in the bottom left corner; the red single and blue double lines represent $w_I = +1$ and -1 ($w_I = +1/2$ and $-1/2$), and the yellow filled circles represent $w_I = 0$ ($w_I = 0$).

At $\gamma \neq 0$, each DP splits into two normal EPs and the corresponding Bloch Hamiltonian $h(k_x, k_y)$ is defective [128–130], generating sixteen EPs at maximum. $h(k_x, k_y)$ has chiral symmetry, which requires the EPs ($E_{\pm} = 0$) on the lines of $k_{x(y)} = \pm\pi/2$ if $t \neq 0$. Although EPs are independent of t , nonzero t is crucial for the existence of isolated EPs. For special system parameters, the hybrid EPs appear at high symmetric points in the Brillouin zone, where normal EPs with the opposite charges merge and the number of EPs reduces.

w_I characterizes the topological features of BTPs as the topological defects of planar vector field $\mathbf{F}(\mathbf{k})$. The value of w_I is given in Fig. 2. Distinct topological phases are created when BTPs merge or split at topological phase transition. Topological phases being reflection symmetric about $\gamma = 0$ has identical w_I configurations, exhibiting seventeen configurations of w_I [Fig. 2].

In Fig. 2, BTPs with $w_I = 0$ are semi-Dirac points on the top panel and are hybrid EPs otherwise. The dispersion is linear along the $k_{x(y)}$ ($k_x = \pm k_y$) direction near the semi-Dirac points on the $k_{x(y)} = \pm\pi/2$ ($k_x = \pm k_y$) line. The dispersion along the $\lambda_1 k_x = \lambda_2 k_y$ ($\lambda_1 k_x = -\lambda_2 k_y$) direction is square-root (linear) near the hybrid EPs ($\lambda_1\pi/2, \lambda_2\pi/2$), where $\lambda_{1,2} = \pm 1$. The dispersion along the $k_x = 0$ ($k_y = 0$) direction is square-root (linear) near the hybrid points ($0, \pm\pi/2$) and $(\pi, \pm\pi/2)$.

Three typical types of vortices for the planar vector

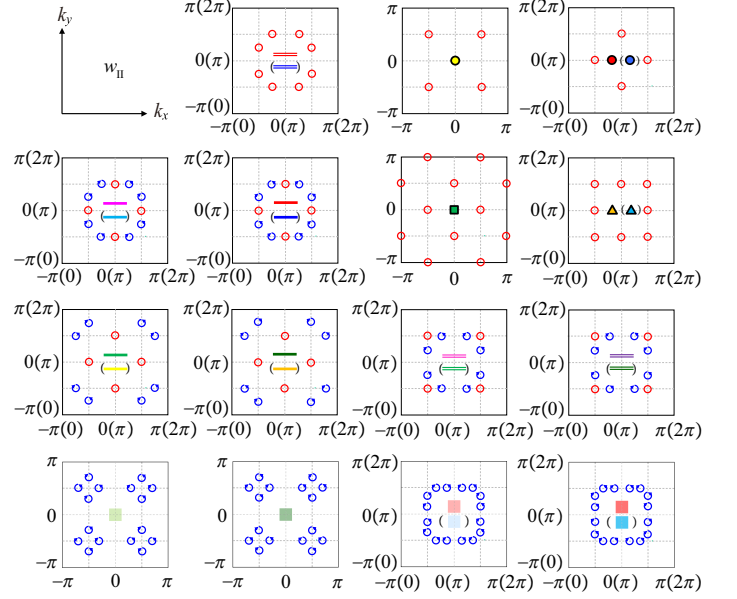


FIG. 3. Schematic of BTP configurations of w_{II} for the topological phases in Fig. 1(b), the corresponding BTP configurations of w_I is in Fig. 2.

fields $\mathbf{F}(\mathbf{k})$ and $\mathbf{E}(\mathbf{k})$ in the bilayer lattice are shown in Fig. 4. The EP configurations are depicted, including both the zero and half-integer vortices of $w_{I,II} = 0$ and $\pm 1/2$ for the EPs. Figures 4(a) and 4(b) include eight one-half vortices (normal EP $w_{I,II} = \pm 1/2$) and four zero vortices (hybrid EP $w_{I,II} = 0$). The three EPs along $k_{y(x)} = -(+)\pi/2$ from $k_{x(y)} = -\pi$ to $k_{x(y)} = +\pi$ have $w_I = \{1/2, 0, -1/2\}$; in contrast, $w_{II} = \{-1/2, 0, +1/2\}$. Figures 4(c) and 4(d) include sixteen one-half vortices (normal EP $w_{I,II} = \pm 1/2$). Figures 4(e) and 4(f) include eight zero vortices (hybrid EP $w_{I,II} = 0$). In essential, the winding numbers w_I and w_{II} reflect the varying directions of planar vector fields $\mathbf{F}(\mathbf{k})$ and $\mathbf{E}(\mathbf{k})$, respectively; they both capture two topological aspects of EPs and provide an overall perspective of the topological properties of non-Hermitian system. w_I reflects the topological properties of system: EPs naturally inherit fractional topological charges from DPs in the Hermitian situation; w_I is a topological invariant that equivalent to the winding number originated from the non-Hermitian generalization of Berry phase that characterizing the varying direction of the effective magnetic field [55, 70, 108].

w_{II} characterizes the chirality of EPs. When $\gamma \rightarrow -\gamma$, the band energy vector becomes $\mathbf{E}'(\mathbf{k}) = (E_x, -E_y)$ with $w_{II}(-\gamma) = -w_{II}(\gamma)$. But w_I is unchanged with $w_I(-\gamma) = w_I(\gamma)$. The phases symmetric about the T -axis in phase diagram [Fig. 1(b)] are two different phases characterized by opposite w_{II} . Thus, all twenty-six BTP configurations of w_{II} distinguish the different topological phases. Compared with the BTP configurations of w_I , the additional nine configurations are attributed to the

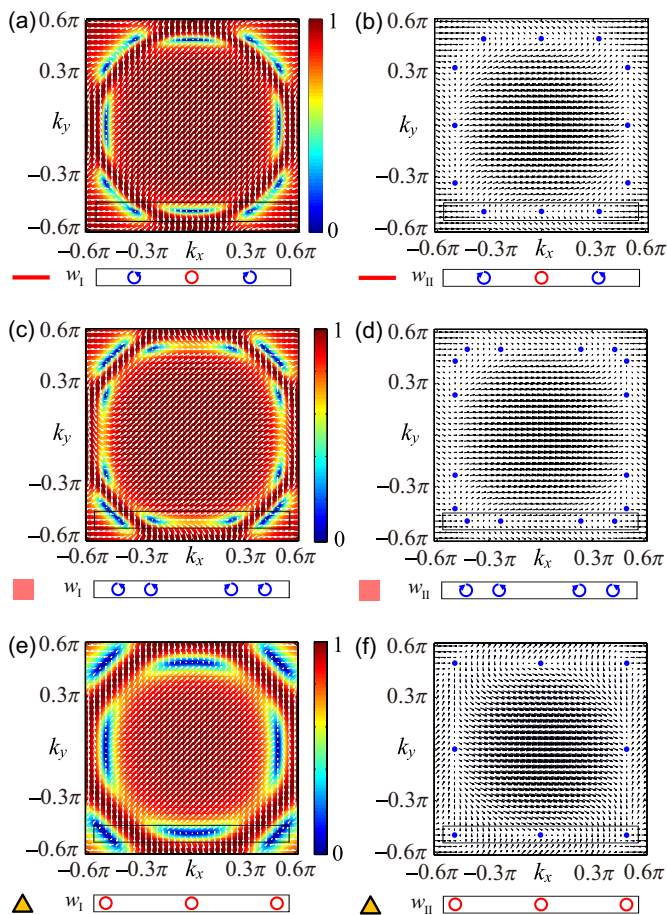


FIG. 4. (a) The planar vector field in the momentum space $\mathbf{F}(\mathbf{k}) = (F_x, F_y) = (\langle \sigma_x \rangle, \langle \sigma_z \rangle)$ is shown by the white arrows on the top, and the background density plot is $F_x^2 + F_y^2$. (b) $\mathbf{E}(\mathbf{k}) = (E_x, E_y) = (\text{Re}(E), \text{Im}(E))$. The plots are for E_+ at system parameters $\gamma = J/2, T = -3J/2$. The vortices in the rectangles are indicated by the winding numbers $w_{I(II)} = +(-)\{+1/2, 0, -1/2\}$ from the left to the right. (c, d) The system parameters are $\gamma = J/2, T = -J$, and (e, f) $\gamma = T = -J$. The winding numbers of EPs inside the rectangles are schematically illustrated at the bottom of each plot.

chirality of EPs that relevant to the positive or negative value of γ . The BTP configurations of w_{II} are shown in Fig. 3 as a supplementary and a comparison to the BTP configurations of w_I of Fig. 2. All different phases are distinguishable in the w_{II} BTP configurations, where the chirality information of EPs are included [18].

The diagonal coupling term t breaks the inversion symmetry and plays a key role in the existence of isolated topologically stable EPs. When $t = 0$, the EPs are no longer isolated points but rings at $\cos k_{cx} + \cos k_{cy} = (-T \pm \gamma) / (2J)$ [27, 76–78, 106, 107, 117, 140, 141]. However, when $t = 0$ and $|\gamma| = |T - 4J|$ ($|T + 4J|$), the EP rings [27] reduce to isolated points at (k_{cx}, k_{cy}) of $k_{cx} = k_{cy} = \pm\pi$ (0) with trivial topological features $w_I = w_{II} = 0$; the real or imaginary part of spectrum in the momentum space possesses a Dirac-cone band struc-

ture for $T > 4J$ or $T < 4J$ ($T < -4J$ or $T > -4J$) at $J > 0$; EP vanishes at $|\gamma| > \max\{|T + 4J|, |T - 4J|\}$ or $|\gamma| < \min\{|T + 4J|, |T - 4J|\}$ if $|T| > 4J$. Recently, the topological features of EP rings are revealed [108, 142].

VI. DISCUSSION AND CONCLUSION

Ultracold atomic gas in optical lattices [109–114, 143–150], photonic crystals [151, 152], and coupled resonators [55, 80, 81, 130, 153–157] provide versatile optical platforms for the study of topological physics; the dissipation and radiation in optical systems are non-Hermitian and thus can be considered as the possible candidate for the experimental realization to the non-Hermitian bilayer square lattice. The fine tuned system parameters are particularly beneficial for the realization of topological systems. Several pioneering experimental and theoretical possibilities have been devoted to ultracold atoms in hexagonal and square optical lattices [158–163]. A particular feature of cold atoms in optical lattice is the tunability of the tunneling strengths. One example is the study of topological quantum phase transition in a bilayer square lattice describing ultracold atomic gases in optical lattices. Trapping cold ^6Li or ^{40}K atoms in a dissipative spin-dependent optical lattice is a candidate for realizing the bilayer square lattice [96, 108–110, 113], and next-nearest-neighbour (diagonal) coupling is introduced by applying additional laser beams. Moreover, the other possible realizations are the coupled resonator waveguide lattice [55, 80, 81, 130, 153–157] and the photonic crystals [151, 152]. The π phase difference between the diagonal couplings t of sublattices A and B is controlled by the optical path length of auxiliary linking resonators (waveguides).

In summary, the symmetry protected isolated EPs in a non-Hermitian system are studied, which differs from the symmetry protected EP rings and EP surfaces [76–78]. A real valued vector field $\mathbf{F}(\mathbf{k})$ is defined by the average values of Pauli matrix. The topological defects of the field are the BTPs associated with the vortices characterized by winding number w_I , which reflects the topological properties of the system. The EPs own fractional topological charges that inherit from their parent DPs in Hermitian systems. The type and number of BTPs is protected by discrete symmetries and only changes at the annihilation or split of vortex and antivortex accompanied by a topological phase transition. A pair of half-integer topological charged EPs can merge into a hybrid EP with vanishing topological charge or a DP with integer topological charge zero or one. Another winding number w_{II} characterizes the chirality of EPs and the Riemann sheet band structure. w_I and w_{II} of EPs provide an overall perspective of the topological properties of the non-Hermitian system and the BTP configurations outline distinct topological phases. Our findings deepen the understanding of symmetry protected non-Hermitian topological phases and may stimulate interest in chasing

for topologically stable EPs in other physical systems.

ACKNOWLEDGMENTS

We acknowledge the support of National Natural Science Foundation of China (Grants No. 11374163 and No. 11605094).

APPENDIX A: SYMMETRY

The mirror-reflection in the x and y directions (M_x and M_y), the translation of one site in the x and y directions (T_x and T_y), the 90 degrees rotation (C_4), and the upper and lower layer interchange (Λ) all change the non-Hermitian bilayer square lattice Hamiltonian $H(J, T, \gamma, t)$ into $H(J, T, -\gamma, -t)$. Therefore, H is invariant under a combination of any two of the above listed operations. For example, a combination operator $\Theta_1 = M_x M_y$ leads to $\Theta_1 H \Theta_1^{-1} = H$; under this symmetry operation, the Bloch Hamiltonian in the momentum space changes into $\Theta_1 h(k_x, k_y) \Theta_1^{-1} = h(-k_x, -k_y)$. Other symmetry $\Theta_2 = \Lambda M_x$ leads to $\Theta_2 H \Theta_2^{-1} = H$; thus, we have $\Theta_2 h(k_x, k_y) \Theta_2^{-1} = h(-k_x, k_y)$. Similarly, set $\Theta_3 = \Lambda M_y$, we have $\Theta_3 h(k_x, k_y) \Theta_3^{-1} = h(k_x, -k_y)$; set $\Theta_4 = M_x C_4$, we have $\Theta_4 h(k_x, k_y) \Theta_4^{-1} = h(k_y, k_x)$; set $\Theta_5 = M_y C_4$, we have $\Theta_5 h(k_x, k_y) \Theta_5^{-1} = h(-k_y, -k_x)$; set $\Theta_6 = \Lambda C_4 M_x M_y$, we have $\Theta_6 h(k_x, k_y) \Theta_6^{-1} = h(k_y, -k_x)$; set $\Theta_7 = C_2$, we have $\Theta_7 h(k_x, k_y) \Theta_7^{-1} = h(-k_x, -k_y)$. These discrete symmetries of the non-Hermitian bilayer square lattice lead to

$$h(k_x, k_y) = h(\pm k_{x(y)}, \pm k_{y(x)}). \quad (\text{A1})$$

Therefore, the number of EPs (DPs) in the bilayer lattice is protected by these symmetries, being invariant unless the topological phase transition occurs when EPs (DPs) merge in the non-Hermitian (Hermitian) bilayer lattice.

APPENDIX B: BTP CONFIGURATION

The complete phase diagram of the bilayer square lattice is illustrated in Fig. 5(a); in contrast to Fig. 1(b), Fig. 5(a) distinguishes all different types of BTP configurations in the system parameter space γ - T . In Figs. 5(b)-5(e), the system parameters are in the colored areas outside the region $|T \pm \gamma| \leq 2$ as a complement of Figs. 2 and 3; notably, all the EPs are still located at $(k_{cx}, \pm\pi/2)$ and $(\pm\pi/2, k_{cy})$ with $|k_{cx(cy)}| = \cos^{-1} [(-T \pm \gamma) / (2J)]$. These topological phases are not discussed in the main text due to the simplicity of this situation. In this situation, eight normal EPs with $w_I = \pm 1/2$ exist as shown on the upper panel of Figs. 5(b) and 5(c), and their mergence creates the new configurations as shown on the upper panel of Figs. 5(d) and 5(e), where four hybrid EPs appear. The BTP configurations for w_{II} outside the

region $|T \pm \gamma| \leq 2$ are depicted on the lower panel of Figs. 5(b)-5(e).

APPENDIX C: DISPERSION NEAR THE BTPS

In this Appendix, we discuss the dispersions near the BTPs (EPs and DPs) with different winding numbers. Here we only discuss the dispersion around EPs at $(k_{cx}, \pm\pi/2)$, and the situations of $(\pm\pi/2, k_{cy})$ can be obtained by interchanging k_x and k_y . Set $q_x = k_x - k_{cx}$ and $q_y = k_y - \pi/2$, the Taylor expansion of the $\mathbf{B}(\mathbf{k})$ field to the second order near $(k_{cx}, \pm\pi/2)$ yields

$$\begin{cases} B_x \approx 2J [(1 - q_x^2/2) \cos k_{cx} - q_x \sin k_{cx} \mp q_y] + T \\ B_y \approx \mp 4tq_y [(1 - q_x^2/2) \cos k_{cx} - q_x \sin k_{cx}] + i\gamma \end{cases}, \quad (\text{C1})$$

and the dispersion is

$$E_{\pm} = \pm \sqrt{B_x^2 + B_y^2}. \quad (\text{C2})$$

In the following, we discuss the dispersion near the EPs and DPs in detail.

Firstly, we consider the dispersion near normal EPs with $w_I = \pm 1/2$. Near $(k_{cx}, \pm\pi/2)$ with $k_{cx} \neq 0, \pi, \pm\pi/2$, we approximately have the dispersion along the $k_y = \xi k_x$ ($k_x = -\xi k_y$) direction as $E_+(k_y = \xi k_x) \approx 2\sqrt{-J(T + 2J \cos k_{cx}) (\sin k_{cx} \pm \xi) \mp 2i\gamma t \xi \cos k_{cx} \sqrt{q_x}}$ and $E_+(k_x = -\xi k_y) \approx 2\sqrt{J(T + 2J \cos k_{cx}) (\xi \sin k_{cx} \mp 1) \mp 2i\gamma t \cos k_{cx} \sqrt{q_y}}$, where ξ is real. Notably, the dispersion along any direction is square-root near normal EPs with $w_I = \pm 1/2$.

Secondly, we consider the dispersion near hybrid EPs with $w_I = 0$. The hybrid points with $w_I = 0$ at $k_{cx} = 0, \pi, \pm\pi/2$ have anisotropic dispersion, being square-root in one direction and linear in the perpendicular direction [70]. For $k_{cx} = \pm\pi/2$ (i.e., $T \pm \gamma = 0$), we approximately have $\mathbf{B}(\mathbf{k})$ field near $(\lambda_1 \pi/2, \lambda_2 \pi/2)$ as

$$\begin{cases} B_x \approx -2J(\lambda_1 q_x + \lambda_2 q_y) + T \\ B_y \approx 4\lambda_1 \lambda_2 t q_x q_y + i\gamma \end{cases}, \quad (\text{C3})$$

where $\lambda_1, \lambda_2 = \pm$. The dispersion along the $\lambda_1 k_x = \lambda_2 k_y$ ($\lambda_1 k_x = -\lambda_2 k_y$) direction is square-root (linear) as

$$E_+(\lambda_1 k_x = \lambda_2 k_y) \approx 2\sqrt{-2\lambda_1 J T \sqrt{q_x}}, \quad (\text{C4})$$

$$E_+(\lambda_1 k_x = -\lambda_2 k_y) \approx 2\sqrt{-2i\gamma t |q_x|}. \quad (\text{C5})$$

For $k_{cx} = 0$ (i.e., $T \pm \gamma = -2J$), we approximately have $\mathbf{B}(\mathbf{k})$ field near $(0, \pm\pi/2)$ as

$$\begin{cases} B_x \approx -J(q_x^2 \pm 2q_y - 2) + T \\ B_y \approx \mp 4tq_y + i\gamma \end{cases}, \quad (\text{C6})$$

and the dispersion along the $k_x = 0$ ($k_y = 0$) direction is square-root (linear) as

$$E_+(k_x = 0) \approx 2\sqrt{\mp J T \mp 2J^2 \mp 2i\gamma t \sqrt{q_y}}, \quad (\text{C7})$$

$$E_+(k_y = 0) \approx \sqrt{-2J T - 4J^2} |q_x|. \quad (\text{C8})$$

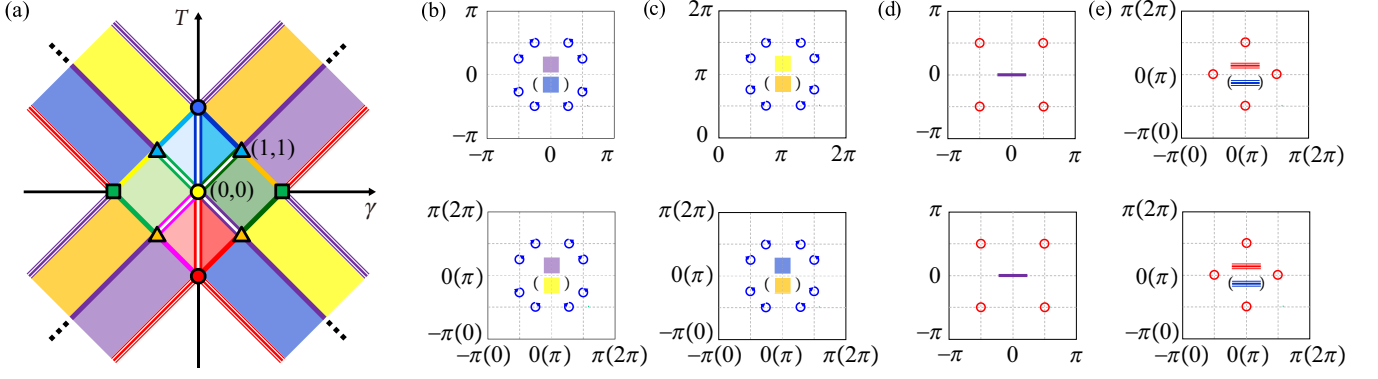


FIG. 5. (a) The phase diagram in the parameter space γ - T . 16 (8) EPs appear in the colored area inside (outside) the region $|T \pm \gamma| \leq 2$, and the system is gapped in the white region. Excepted for the whole twenty-six BTP configurations shown in Figs. 2 and 3, other BTP configurations outside the region $|T \pm \gamma| \leq 2$ are illustrated in (b-e). The upper (lower) panel is the configurations of w_I (w_{II}).

For $k_{cx} = \pi$ (i.e., $T \pm \gamma = 2J$), we approximately have $\mathbf{B}(\mathbf{k})$ field near $(\pi, \pm\pi/2)$ as

$$\begin{cases} B_x \approx J(q_x^2 \mp 2q_y - 2) + T \\ B_y \approx \pm 4tq_y + i\gamma \end{cases}, \quad (\text{C9})$$

and the dispersion along the $k_x = 0$ ($k_y = 0$) direction is square-root (linear) as

$$E_+(k_x = 0) \approx 2\sqrt{\mp JT \pm 2J^2 \pm 2i\gamma t\sqrt{q_y}}, \quad (\text{C10})$$

$$E_+(k_y = 0) \approx \sqrt{2JT - 4J^2} |q_x|. \quad (\text{C11})$$

Thirdly, the system is Hermitian at $\gamma = 0$ and the BTPs are DPs. The dispersion near the DPs with $w_I = 0$ is anisotropy, being linear along one direction and quadratic along the perpendicular direction. DPs here are semi-Dirac points [123]. For $k_{cx} = \pm\pi/2$ (i.e., $T = 0$), we approximately have $\mathbf{B}(\mathbf{k})$ field near $(\lambda_1\pi/2, \lambda_2\pi/2)$ as

$$\begin{cases} B_x \approx -2J(\lambda_1 q_x + \lambda_2 q_y) \\ B_y \approx 4\lambda_1 \lambda_2 t q_x q_y \end{cases}, \quad (\text{C12})$$

and the dispersion along the $\lambda_1 k_x = \lambda_2 k_y$ ($\lambda_1 k_x = -\lambda_2 k_y$) direction is linear (quadratic) as

$$E_+(\lambda_1 k_x = \lambda_2 k_y) \approx 4J |q_x|, \quad (\text{C13})$$

$$E_+(\lambda_1 k_x = -\lambda_2 k_y) \approx 4tq_x^2. \quad (\text{C14})$$

For $k_{cx} = 0$ (i.e., $T = -2J$), we approximately have $\mathbf{B}(\mathbf{k})$ field near $(0, \pm\pi/2)$ as

$$\begin{cases} B_x \approx -J(q_x^2 \pm 2q_y) \\ B_y \approx \mp 4tq_y \end{cases}, \quad (\text{C15})$$

and the dispersion along the $k_x = 0$ ($k_y = 0$) direction is linear (quadratic) as

$$E_+(k_x = 0) \approx 2\sqrt{J^2 + 4t^2} |q_y|, \quad (\text{C16})$$

$$E_+(k_y = 0) \approx Jq_x^2. \quad (\text{C17})$$

For $k_{cx} = \pi$ (i.e., $T = 2J$), we approximately have $\mathbf{B}(\mathbf{k})$ field near $(\pi, \pm\pi/2)$ as

$$\begin{cases} B_x \approx J(q_x^2 \mp 2q_y) \\ B_y \approx \pm 4tq_y \end{cases}, \quad (\text{C18})$$

and the dispersion along the $k_x = 0$ ($k_y = 0$) direction is linear (quadratic) as

$$E_+(k_x = 0) \approx 2\sqrt{J^2 + 4t^2} |q_y|, \quad (\text{C19})$$

$$E_+(k_y = 0) \approx Jq_x^2. \quad (\text{C20})$$

Fourthly, we consider the dispersion near DPs with $w_I = \pm 1$. Near $(k_{cx}, \pm\pi/2)$ with $k_{cx} \neq 0, \pi, \pm\pi/2$, we approximately have $\mathbf{B}(\mathbf{k})$ field as

$$\begin{cases} B_x \approx 2J(-q_x \sin k_{cx} \mp q_y) \\ B_y \approx \mp 4tq_y \cos k_{cx} \end{cases}, \quad (\text{C21})$$

and the dispersion along the $k_y = \xi k_x$ ($k_x = -\xi k_y$) direction is

$$\begin{aligned} E_+(k_y = \xi k_x) &\approx 2\sqrt{J^2 (\sin k_{cx} \pm \xi)^2 + 4t^2 \xi^2 \cos^2 k_{cx}} |q_x| \\ E_+(k_x = -\xi k_y) &\approx 2\sqrt{J^2 (\xi \sin k_{cx} \mp 1)^2 + 4t^2 \cos^2 k_{cx}} |q_y| \end{aligned} \quad (\text{C22})$$

Notably, DPs with $w_I = \pm 1$ have linear dispersion along any direction; DPs here are Dirac points.

REFERENCES

-
- [1] N. Moiseyev, *Non-Hermitian Quantum Mechanics* (Cambridge Univ. Press, 2011).
- [2] C. M. Bender, Rep. Prog. Phys. **70**, 947 (2007).
- [3] I. Rotter, J. Phys. A **42**, 153001 (2009).
- [4] W. D. Heiss, J. Phys. A **45**, 444016 (2012).
- [5] H. Cao and J. Wiersig, Rev. Mod. Phys. **87**, 61 (2015).
- [6] Z. H. Musslimani, K. G. Makris, R. El-Ganainy, and D. N. Christodoulides, Phys. Rev. Lett. **100**, 030402 (2008).
- [7] A. Guo, G. J. Salamo, D. Duchesne, R. Morandotti, M. Volatier-Ravat, V. Aimez, G. A. Siviloglou, and D. N. Christodoulides, Phys. Rev. Lett. **103**, 093902 (2009).
- [8] B. Peng, S. K. Ozdemir, F. Lei, F. Monifi, M. Gianfreda, G. L. Long, S. Fan, F. Nori, C. M. Bender, and L. Yang, Nat. Phys. **10**, 394 (2014).
- [9] L. Chang, X. Jiang, S. Hua, C. Yang, J. Wen, L. Jiang, G. Li, G. Wang, and M. Xiao, Nat. Photon. **8**, 524 (2014).
- [10] Z. Zhang, Y. Zhang, J. Sheng, L. Yang, M.-A. Miri, D. N. Christodoulides, B. He, Y. Zhang, and M. Xiao, Phys. Rev. Lett. **117**, 123601 (2016).
- [11] L. Feng, R. El-Ganainy, and L. Ge, Nat. Photon. **11**, 752 (2017).
- [12] S. Longhi, Eur. Phys. Lett. **120**, 64001 (2017).
- [13] Y. Huang, Y. Shen, C. Min, S. Fan, and G. Veronis, Nanophotonics **6**, 977 (2017).
- [14] L. Jin and Z. Song, Phys. Rev. Lett. **121**, 073901 (2018).
- [15] R. El-Ganainy, K. G. Makris, M. Khajavikhan, Z. H. Musslimani, S. Rotter, and D. N. Christodoulides, Nat. Phys. **14**, 11 (2018).
- [16] S. K. Gupta, Y. Zou, X. Y. Zhu, M. H. Lu, L. Zhang, X. P. Liu, and Y. F. Chen, arXiv:1803.00794.
- [17] W. D. Heiss and H. L. Harney, Eur. Phys. J. D **17**, 149 (2001).
- [18] C. Dembowski, H.-D. Gräf, H. L. Harney, A. Heine, W. D. Heiss, H. Rehfeld, and A. Richter, Phys. Rev. Lett. **86**, 787 (2001).
- [19] C. Dembowski, B. Dietz, H.-D. Gräf, H. L. Harney, A. Heine, W. D. Heiss, and A. Richter, Phys. Rev. Lett. **90**, 034101 (2003).
- [20] C. Dembowski, B. Dietz, H.-D. Gräf, H. L. Harney, A. Heine, W. D. Heiss, and A. Richter, Phys. Rev. E **69**, 056216 (2004).
- [21] C. E. Rüter, K. G. Makris, R. El-Ganainy, D. N. Christodoulides, M. Segev, and D. Kip, Nat. Phys. **6**, 192 (2010).
- [22] J. Wiersig, Phys. Rev. Lett. **112**, 203901 (2014).
- [23] W. Chen, S. K. Ozdemir, G. Zhao, J. Wiersig, and L. Yang, Nature **548**, 192 (2017).
- [24] H. Hodaie, A. U. Hassan, S. Wittek, H. Garcia-Gracia, R. El-Ganainy, D. N. Christodoulides, and M. Khajavikhan, Nature **548**, 187 (2017).
- [25] S. Lin, X. Z. Zhang, C. Li, and Z. Song, Phys. Rev. A **94**, 042133 (2016).
- [26] R. Uzdin, A. Mailybaev, and N. Moiseyev, J. Phys. A **44**, 435302 (2011).
- [27] B. Zhen, C. W. Hsu, Y. Igarashi, L. Lu, I. Kaminer, A. Pick, S.-L. Chua, J. D. Joannopoulos, and M. Soljačić, Nature **525**, 354 (2015).
- [28] J. Doppler, A. A. Mailybaev, J. Böhm, U. Kuhl, A. Girschik, F. Libisch, T. J. Milburn, P. Rabl, N. Moiseyev, and S. Rotter, Nature **537**, 76 (2016).
- [29] H. Xu, D. Mason, L. Jiang, and J. G. E. Harris, Nature **537**, 80 (2016).
- [30] D. Heiss, Nat. Phys. **12**, 823 (2016).
- [31] A. U. Hassan, B. Zhen, M. Soljačić, M. Khajavikhan, and D. N. Christodoulides, Phys. Rev. Lett. **118**, 093002 (2017).
- [32] M. V. Berry, Czech. J. Phys. **54**, 1039 (2004).
- [33] A. A. Mailybaev, O. N. Kirillov, and A. P. Seyranian, Phys. Rev. A **72**, 014104 (2005).
- [34] M. Müller and I. Rotter, J. Phys. A: Math. Theor. **41**, 244018 (2008).
- [35] S.-D. Liang and G.-Y. Huang, Phys. Rev. A **87**, 012118 (2013).
- [36] K. Ding, G. Ma, M. Xiao, Z. Q. Zhang, and C. T. Chan, Phys. Rev. X **6**, 021007 (2016).
- [37] X.-L. Zhang, S. Wang, B. Hou, and C. T. Chan, Phys. Rev. X **8**, 021066 (2018).
- [38] L. Jin, Phys. Rev. A **97**, 012121 (2018).
- [39] D. S. Borgnia, A. J. Kruchkov, and R. J. Slager, arXiv:1902.07217.
- [40] H. Zhou and J. Y. Lee, arXiv:1812.10490.
- [41] M. Ezawa, arXiv:1810.04527; arXiv:1811.12059; arXiv:1902.03716.
- [42] Y. C. Hu and T. L. Hughes, Phys. Rev. B **84**, 153101 (2011).
- [43] K. Esaki, M. Sato, K. Hasebe, and M. Kohmoto, Phys. Rev. B **84**, 205128 (2011).
- [44] G. Q. Liang and Y. D. Chong, Phys. Rev. Lett. **110**, 203904 (2013).
- [45] H. Schomerus, Opt. Lett. **38**, 1912 (2013).
- [46] B. Zhu, R. Lü, and S. Chen, Phys. Rev. A **89**, 062102 (2014).
- [47] J. M. Zeuner, M. C. Rechtsman, Y. Plotnik, Y. Lumer, S. Nolte, M. S. Rudner, M. Segev, and A. Szameit, Phys. Rev. Lett. **115**, 040402 (2015).
- [48] C. Yuce, Phys. Lett. A **379**, 1213 (2015).
- [49] X. Wang, T. Liu, Y. Xiong, and P. Tong, Phys. Rev. A **92**, 012116 (2015).
- [50] C. Poli, M. Bellec, U. Kuhl, F. Mortessagne, and H. Schomerus, Nat. Commun. **6**, 6710 (2015).
- [51] S. Malzard, C. Poli, and H. Schomerus, Phys. Rev. Lett. **115**, 200402 (2015).
- [52] T. E. Lee, Phys. Rev. Lett. **116**, 133903 (2016).
- [53] C. He, X. C. Sun, X. P. Liu, M. H. Lu, Y. Chen, L. Feng, and Y. F. Chen, Proc. Natl. Acad. Sci. USA. **113**, 4924 (2016).
- [54] S. Weimann, M. Kremer, Y. Plotnik, Y. Lumer, S. Nolte, K. G. Makris, M. Segev, M. C. Rechtsman, and A. Szameit, Nat. Mater. **16**, 433 (2017).
- [55] D. Leykam, K. Y. Bliokh, C. Huang, Y. D. Chong, and F. Nori, Phys. Rev. Lett. **118**, 040401 (2017).
- [56] Y.-X. Xiao, G. Ma, Z.-Q. Zhang, and C. T. Chan, Phys. Rev. Lett. **118**, 166803 (2017).
- [57] L. Jin, P. Wang, and Z. Song, Sci. Rep. **7**, 5903 (2017).
- [58] L. Jin, Phys. Rev. A **96**, 032103 (2017).
- [59] M. Klett, H. Cartarius, D. Dast, J. Main, and G. Wunner, Phys. Rev. A **95**, 053626 (2017).
- [60] S. Lieu, Phys. Rev. B **97**, 045106 (2018).
- [61] M. Pan, H. Zhao, P. Miao, S. Longhi, and L. Feng, Nat. Commun. **9**, 1308 (2018).

- [62] W. Zhu, X. Fang, D. Li, Y. Sun, Y. Li, Y. Jing, and H. Chen, *Phys. Rev. Lett.* **121**, 124501 (2018).
- [63] J. Hou, Z. Li, X.-W. Luo, Q. Gu, and C. Zhang, arXiv:1808.06972.
- [64] Z. Yang and J. Hu, *Phys. Rev. B*, **99**, 081102(R) (2019).
- [65] H. Wang, J. Ruan, and H. Zhang, *Phys. Rev. B* **99**, 075130 (2019).
- [66] K. Kawabata, S. Higashikawa, Z. Gong, Y. Ashida, and M. Ueda, *Nat. Commun.* **10**, 297 (2019).
- [67] K. Kawabata, K. Shiozaki, M. Ueda, and M. Sato, arXiv:1812.09133.
- [68] Y. Xiong, *J. Phys. Commun.* **2**, 035043 (2018).
- [69] C. Yin, H. Jiang, L. Li, R. Lü, and S. Chen, *Phys. Rev. A* **97**, 052115 (2018).
- [70] H. Shen, B. Zhen, and L. Fu, *Phys. Rev. Lett.* **120**, 146402 (2018).
- [71] S. Yao and Z. Wang, *Phys. Rev. Lett.* **121**, 086803 (2018).
- [72] S. Yao, F. Song, and Z. Wang, *Phys. Rev. Lett.* **121**, 136802 (2018).
- [73] Z. Gong, Y. Ashida, K. Kawabata, K. Takasan, S. Higashikawa, and M. Ueda, *Phys. Rev. X* **8**, 031079 (2018).
- [74] F. K. Kunst, E. Edvardsson, J. C. Budich, and E. J. Bergholtz, *Phys. Rev. Lett.* **121**, 026808 (2018).
- [75] L. Jin and Z. Song, *Phys. Rev. B* **99**, 081103(R) (2019).
- [76] J. C. Budich, J. Carlström, F. K. Kunst, and E. J. Bergholtz, *Phys. Rev. B* **99**, 041406(R) (2019).
- [77] R. Okugawa and T. Yokoyama, *Phys. Rev. B* **99**, 041202(R) (2019).
- [78] T. Yoshida, R. Peters, N. Kawakami, and Y. Hatsugai, *Phys. Rev. B* **99**, 121101(R) (2019).
- [79] H. Zhou, J. Y. Lee, S. Liu, and B. Zhen, *Optica* **6**, 190 (2019).
- [80] H. Zhao, P. Miao, M. H. Teimourpour, S. Malzard, R. El-Ganainy, H. Schomerus, and L. Feng, *Nat. Commun.* **9**, 981 (2018).
- [81] M. Parto, S. Wittek, H. Hodaei, G. Harari, M. A. Bandres, J. Ren, M. C. Rechtsman, M. Segev, D. N. Christodoulides, and M. Khajavikhan, *Phys. Rev. Lett.* **120**, 113901 (2018).
- [82] G. Harari, M. A. Bandres, Y. Lumer, M. C. Rechtsman, Y. D. Chong, M. Khajavikhan, D. N. Christodoulides, and M. Segev, *Science* **359**, eaar4003 (2018).
- [83] M. A. Bandres, S. Wittek, G. Harari, M. Parto, J. Ren, M. Segev, D. Christodoulides, and M. Khajavikhan, *Science* **359**, eaar4005 (2018).
- [84] P. St-Jean, V. Goblot, E. Galopin, A. Lemaître, T. Ozawa, L. Le Gratiet, I. Sagnes, J. Bloch, and A. Amo, *Nat. Photon.* **11**, 651 (2017).
- [85] M. V. Berry and M. Wilkinson, *Proc. R. Soc. A* **392**, 15 (1984).
- [86] X. Wan, A. M. Turner, A. Vishwanath, and S. Y. Savrasov, *Phys. Rev. B* **83**, 205101 (2011).
- [87] K. Y. Yang, Y. M. Lu, and Y. Ran, *Phys. Rev. B* **84**, 075129 (2011).
- [88] A. A. Burkov and L. Balents, *Phys. Rev. Lett.* **107**, 127205 (2011).
- [89] G. Xu, H. Weng, Z. Wang, X. Dai, and Z. Fang, *Phys. Rev. Lett.* **107**, 186806 (2011).
- [90] W. Witczak-Krempa and Y. B. Kim, *Phys. Rev. B* **85**, 045124 (2012).
- [91] H. Weng, C. Fang, Z. Fang, B. A. Bernevig, and X. Dai, *Phys. Rev. X* **5**, 011029 (2015).
- [92] S.-M. Huang, S.-Y. Xu, I. Belopolski, C.-C. Lee, G. Chang, B. K. Wang, N. Alidoust, G. Bian, M. Neupane, C. Zhang, S. Jia, A. Bansil, H. Lin, and M. Z. Hasan, *Nat. Commun.* **6**, 7373 (2015).
- [93] S. M. Young, S. Zaheer, J. C. Y. Teo, C. L. Kane, E. J. Mele, and A. M. Rappe, *Phys. Rev. Lett.* **108**, 140405 (2012).
- [94] Z. Wang, Y. Sun, X.-Q. Chen, C. Franchini, G. Xu, H. Weng, X. Dai, and Z. Fang, *Phys. Rev. B* **85**, 195320 (2012).
- [95] Z. Wang, H. Weng, Q. Wu, X. Dai, and Z. Fang, *Phys. Rev. B* **88**, 125427 (2013).
- [96] K. Sun, W. V. Liu, A. Hemmerich, and S. Das Sarma, *Nat. Phys.* **8**, 67 (2012).
- [97] J. M. Hou, *Phys. Rev. Lett.* **111**, 130403 (2013).
- [98] Z. K. Liu, B. Zhou, Y. Zhang, Z. J. Wang, H. M. Weng, D. Prabhakaran, S.-K. Mo, Z. X. Shen, Z. Fang, X. Dai, Z. Hussain, and Y. L. Chen, *Science* **343**, 864 (2014).
- [99] M. Neupane, S.-Y. Xu, R. Sankar, N. Alidoust, G. Bian, C. Liu, I. Belopolski, T.-R. Chang, H.-T. Jeng, H. Lin, A. Bansil, F. Chou, and M. Z. Hasan, *Nat. Commun.* **5**, 3786 (2014).
- [100] S.-Y. Xu, I. Belopolski, N. Alidoust, M. Neupane, C. Zhang, R. Sankar, S.-M. Huang, C.-C. Lee, G. Chang, B. K. Wang, G. Bian, H. Zheng, D. S. Sanchez, F. Chou, H. Lin, S. Jia, and M. Z. Hasan, *Science* **349**, 613 (2015).
- [101] B. Q. Lv, H. M. Weng, B. B. Fu, X. P. Wang, H. Miao, J. Ma, P. Richard, X. C. Huang, L. X. Zhao, G. F. Chen, Z. Fang, X. Dai, T. Qian, and H. Ding, *Phys. Rev. X* **5**, 031013 (2015).
- [102] L. Lu, Z. Wang, D. Ye, L. Ran, L. Fu, J. D. Joannopoulos, and M. Soljačić, *Science* **349**, 622 (2015).
- [103] K. Ding, Z. Q. Zhang, and C. T. Chan, *Phys. Rev. B* **92**, 235310 (2015).
- [104] M. Xiao, G. Ma, Z. Yang, P. Sheng, Z. Q. Zhang, and C. T. Chan, *Nat. Phys.* **11**, 240 (2015).
- [105] J.-M. Hou, *Phys. Rev. B* **89**, 235405 (2014).
- [106] A. Szameit, M. C. Rechtsman, O. Bahat-Treidel, and M. Segev, *Phys. Rev. A* **84**, 021806(R) (2011).
- [107] A. Cerjan, A. Raman, and S. Fan, *Phys. Rev. Lett.* **116**, 203902 (2016).
- [108] Y. Xu, S.-T. Wang, and L.-M. Duan, *Phys. Rev. Lett.* **118**, 045701 (2017).
- [109] S. Diehl, A. Micheli, A. Kantian, B. Kraus, H. P. Büchler, and P. Zoller, *Nat. Phys.* **4**, 878 (2008).
- [110] F. Verstraete, M. M. Wolf, and J. I. Cirac, *Nat. Phys.* **5**, 633 (2009).
- [111] S. Diehl, E. Rico, M. A. Baranov, and P. Zoller, *Nat. Phys.* **7**, 971 (2011).
- [112] C.-E. Bardyn, M. A. Baranov, E. Rico, A. İmamoğlu, P. Zoller, and S. Diehl, *Phys. Rev. Lett.* **109**, 130402 (2012).
- [113] C.-E. Bardyn, M. A. Baranov, C. V. Kraus, E. Rico, A. İmamoğlu, P. Zoller, and S. Diehl, *New J. Phys.* **15**, 085001 (2013).
- [114] J. C. Budich, P. Zoller, and S. Diehl, *Phys. Rev. A* **91**, 042117 (2015).
- [115] Under definitions $\vec{\sigma}' = (\sigma_z, \sigma_x, \sigma_y)$, $\mathbf{B}'(\mathbf{k}) = (B'_x, B'_y, 0)$ with $B'_{x(y)} = B_{y(x)}$, and $\mathbf{F}'(\mathbf{k}) = (\langle\sigma_z\rangle, \langle\sigma_x\rangle)$, $w'_1 (w_1)$ calculated from $\mathbf{F}'(\mathbf{k})$ [$\mathbf{F}(\mathbf{k})$] is consistent with that in Ref. [55] ([96]) and $w'_1 = -w_1$.
- [116] A. P. Schnyder, S. Ryu, A. Furusaki, and A. W. W. Ludwig, *Phys. Rev. B* **78**, 195125 (2008).
- [117] S. Lin and Z. Song, *Phys. Rev. A* **96**, 052121 (2017).

- [118] L. Fu and C. L. Kane, Phys. Rev. B **76**, 045302 (2007).
- [119] P. Dietl, F. Piéchon, and G. Montambaux, Phys. Rev. Lett. **100**, 236405 (2008).
- [120] S. Banerjee, R. R. P. Singh, V. Pardo, and W. E. Pickett, Phys. Rev. Lett. **103**, 016402 (2009).
- [121] J. Kim, S. S. Baik, S. H. Ryu, Y. Sohn, S. Park, B.-G. Park, J. Denlinger, Y. Yi, H. J. Choi, and K. S. Kim, Science **349**, 723 (2015).
- [122] L. Du, X. Zhou, and G. A. Fiete, Phys. Rev. B **95**, 035136 (2017).
- [123] Q. Chen, L. Du, and G. A. Fiete, Phys. Rev. B **97**, 035422 (2018).
- [124] K. Sun, H. Yao, E. Fradkin, and S. A. Kivelson, Phys. Rev. Lett. **103**, 046811 (2009).
- [125] G. Montambaux, F. Piéchon, J.-N. Fuchs, and M. O. Goerbig, Phys. Rev. B **80**, 153412 (2009).
- [126] L.-K. Lim, J.-N. Fuchs, and G. Montambaux, Phys. Rev. Lett. **108**, 175303 (2012).
- [127] L. Tarruell, D. Greif, T. Uehlinger, G. Jotzu, and T. Esslinger, Nature **483**, 302 (2012).
- [128] F. Keck, H. J. Korsch, and S. Mossmann, J. Phys. A: Math. Gen. **36**, 2125 (2003).
- [129] O. N. Kirillov, A. A. Mailybaev, and A. P. Seyranian, J. Phys. Math. Gen. **38**, 5531 (2005).
- [130] H. Zhou, C. Peng, Y. Yoon, C. W. Hsu, K. A. Nelson, L. Fu, J. D. Joannopoulos, M. Soljačić, and B. Zhen, Science **359**, 1009 (2018).
- [131] T. H. Hsieh, H. Lin, J. Liu, W. Duan, A. Bansil, and L. Fu, Nat. Commun. **3**, 982 (2012).
- [132] Q. Lin, M. Xiao, L. Yuan, and S. Fan, Nat. Commun. **7**, 13731 (2016).
- [133] S. M. Young, S. Zaheer, J. C. Y. Teo, C. L. Kane, E. J. Mele, and A. M. Rappe, Phys. Rev. Lett. **108**, 140405 (2012).
- [134] S. A. Yang, H. Pan, and F. Zhang, Phys. Rev. Lett. **113**, 046401 (2014).
- [135] A. A. Burkov and L. Balents, Phys. Rev. Lett. **107**, 127205 (2011).
- [136] G. B. Halász and L. Balents, Phys. Rev. B **85**, 035103 (2012).
- [137] L. Lu, Z. Wang, D. Ye, L. Ran, L. Fu, J. D. Joannopoulos, and M. Soljačić, Science, **349**, 622 (2015).
- [138] B. Q. Lv, N. Xu, H. M. Weng, J. Z. Ma, P. Richard, X. C. Huang, L. X. Zhao, G. F. Chen, C. E. Matt, F. Bisti, V. N. Strocov, J. Mesot, Z. Fang, X. Dai, T. Qian, M. Shi, and H. Ding, Nat. Phys. **11**, 724 (2015).
- [139] The topological band structure determines the EP chirality, which is relevant to the coalescence eigenstate. In Fig. 4(b), w_{II} from left to right are $+(-)\{-1/2, 0, +1/2\}$ when $\gamma > 0$ ($\gamma < 0$); however, the two outer EPs have the identical coalescence state.
- [140] Y. Xu and C. Zhang, Phys. Rev. A **93**, 063606 (2016).
- [141] D.-W. Zhang, Y. X. Zhao, R.-B. Liu, Z.-Y. Xue, S.-L. Zhu, and Z. D. Wang, Phys. Rev. A **93**, 043617 (2016).
- [142] A. Cerjan, M. Xiao, L. Yuan, and S. Fan, Phys. Rev. B **97**, 075128 (2018).
- [143] S.-L. Zhu, B. Wang, and L.-M. Duan, Phys. Rev. Lett. **98**, 260402 (2007).
- [144] I. Bloch, J. Dalibard, and W. Zwerger, Rev. Mod. Phys. **80**, 885 (2008).
- [145] X.-J. Liu, K. T. Law, T. K. Ng, and P. A. Lee, Phys. Rev. Lett. **111**, 120402 (2013).
- [146] M. Aidelsburger, M. Atala, M. Lohse, J. T. Barreiro, B. Paredes, and I. Bloch, Phys. Rev. Lett. **111**, 185301 (2013).
- [147] X.-J. Liu, K. T. Law, and T. K. Ng, Phys. Rev. Lett. **112**, 086401 (2014).
- [148] M. Aidelsburger, M. Lohse, C. Schweizer, M. Atala, J. T. Barreiro, S. Nascimbène, N. R. Cooper, I. Bloch, and N. Goldman, Nat. Phys. **11**, 162 (2015).
- [149] Z. Wu, L. Zhang, W. Sun, X.-T. Xu, B.-Z. Wang, S.-C. Ji, Y. Deng, S. Chen, X.-J. Liu, and J.-W. Pan, Science **354**, 83 (2016).
- [150] N. Goldman, J. C. Budich, and P. Zoller, Nat. Phys. **12**, 639 (2016).
- [151] S. A. Skirlo, L. Lu, Y. Igarashi, Q. Yan, J. Joannopoulos, and M. Soljačić, Phys. Rev. Lett. **115**, 253901 (2015).
- [152] S. Mittal, S. Ganeshan, J. Fan, A. Vaez, and M. Hafezi, Nat. Photon. **10**, 180 (2016).
- [153] M. Hafezi, E. A. Demler, M. D. Lukin, and J. M. Taylor, Nat. Phys. **7**, 907 (2011).
- [154] K. Fang, Z. Yu, and S. Fan, Nat. Photon. **6**, 782 (2012).
- [155] L. Lu, J. D. Joannopoulos, and M. Soljačić, Nat. Photon. **8**, 821 (2014).
- [156] D. Leykam, M. C. Rechtsman, and Y. D. Chong, Phys. Rev. Lett. **117**, 013902 (2016).
- [157] Q. Lin, M. Xiao, L. Yuan, and S. Fan, Nat. Commun. **7**, 13731 (2016).
- [158] M. A. Baranov, M. Dalmonte, G. Pupillo, and P. Zoller, Chem. Rev. **112**, 5012 (2012).
- [159] P. Soltan-Panahi, J. Struck, P. Hauke, A. Bick, W. Plenkers, G. Meineke, C. Becker, P. Windpassinger, M. Lewenstein, and K. Sengstock, Nat. Phys. **7**, 434 (2011).
- [160] T. Graß, R. W. Chhajlany, L. Tarruell, V. Pellegrini, and M. Lewenstein, 2D Mater. **4**, 015039 (2017).
- [161] C. Gross and I. Bloch, Science **357**, 995 (2017).
- [162] D. Barredo, V. Lienhard, S. de Léséleuc, T. Lahaye, and A. Browaeys, Nature **561**, 79 (2018).
- [163] S. Yoo, New J. Phys. **20**, 083012 (2018).